Nutrient availability and senescence spatially structure the dynamics of a foundation species

Tom W. Bell[a,b,1] and David A. Siegel[b,c]

[a]Department of Applied Ocean Physics and Engineering, Woods Hole Oceanographic Institution, Woods Hole, MA 02543; [b]Earth Research Institute, University of California, Santa Barbara, CA 93106; and [c]Department of Geography, University of California, Santa Barbara, CA 93106

Edited by Matthew Edwards, Biology, San Diego State University, San Diego, CA; received March 21, 2021; accepted November 11, 2021 by Editorial Board Member James A. Estes

Disentangling the roles of the external environment and internal biotic drivers of plant population dynamics is challenging due to the absence of relevant physiological and abundance information over appropriate space and time scales. Remote observations of giant kelp biomass and photosynthetic pigment concentrations are used to show that spatiotemporal patterns of physiological condition, and thus growth and production, are regulated by different processes depending on the scale of observation. Nutrient supply was linked to regional scale (>1 km) physiological condition dynamics, and kelp forest stands were more persistent where nutrient levels were consistently high. However, on local scales (<1 km), internal senescence processes related to canopy age demographics determined patterns of biomass loss across individual kelp forests despite uniform nutrient conditions. Repeat measurements of physiology over continuous spatial fields can provide insights into complex dynamics that are unexplained by the environmental drivers thought to regulate abundance. Emerging remote sensing technologies that provide simultaneous estimates of abundance and physiology can quantify the roles of environmental change and demographics governing plant population dynamics for a wide range of aquatic and terrestrial ecosystems.

physiology | population | biomass | hyperspectral | giant kelp

Ecological population dynamics are driven by the interplay of the external environment and intrinsic biotic factors, which are often difficult to disentangle, especially when observing the system over a single or limited range of scales (1, 2). Since landscapes exist as a mosaic of patches (3) across environmental gradients (4), predictions on how populations respond to changes in the environment tend to be scale dependent (5). Plant responses to broad-scale environmental drivers (e.g., sunlight, nutrients, and disturbance) occur simultaneously with biotic processes such as stomatal conductance, reproduction, and senescence, which operate on the scale of the organism (6). Senescence is the progressive and irreversible deterioration in an organism's physiological performance (7) and can induce synchronous mortality of plant organs or individuals (8), especially in the absence of destructive external factors such as disturbance (9). While the longevity of plant structures has evolved to optimize photosynthetic gains (10), the retention or loss of conspicuous structures may, at times, defy expectations when only environmental factors are considered. For example, field measurements showed that the leaf area index of a single mangrove species decreased as a function of stand age across an area with uniform environmental conditions (~30 km; ref. 11). Since leaf area index underpins the determination of terrestrial net primary production (12), local variability in ecosystem function may be more closely related to age demographics, which are often the result of patchy recruitment patterns (13). However, since field measurements are often discrete and occur over small scales, teasing apart how the environment and age demographics influence plant populations has been difficult across ecosystems due to an absence of relevant measurements over large continuous spatial scales (14, 15). Understanding the scale of senescence and demographic processes across patches and their interaction with broad-scale physical drivers is important to predict how plant populations will respond to environmental change.

Spaceborne imaging spectroscopy has the potential to simultaneously deliver global estimates of plant abundance and physiological condition dynamics at ecologically relevant spatial scales (~30 m). The numerous and contiguous spectral measurements from each image pixel can be used to estimate a variety of physiological metrics, such as pigment content and composition and foliar chemistry, while maintaining the ability to provide the estimates of abundance assessed by existing satellite sensors (16). Quantifying the physiological condition dynamics of terrestrial and aquatic primary producers using spaceborne imaging spectroscopy has been identified as a key research objective for Earth observation in the coming decade (17). In preparation for a nascent spaceborne imaging spectrometer, many high-altitude aerial missions provided repeat imaging spectrometer data covering several terrestrial and aquatic ecosystems (18).

The globally distributed macroalga giant kelp (*Macrocystis pyrifera*) is a superb model organism to examine the relative roles of the external environment and internal biotic factors on abundance dynamics across vast spatial and temporal scales. The conspicuous monoculture surface canopy of giant kelp is amenable to remote measurement (19), and its rapid growth

Significance

Landscapes are spatially heterogeneous, and the measurement of spatial pattern is dependent upon observation scale. Understanding plant populations requires assessing their extrinsic interactions with the environment as well as intrinsic biological processes and has been difficult because of the inability to track both plant abundance and health on appropriate scales. We introduce remote sensing observations that assess the abundance and health of giant kelp, an important ecosystem-structuring species, over regional and local scales. We find that both extrinsic nutrient availability and intrinsic senescence processes regulate population dynamics but on regional and local scales, respectively. This suggests that future satellite missions will be able to assess plant abundance and health and their interactions with the environment on local to global scales.

Author contributions: T.W.B. and D.A.S. designed research; T.W.B. performed research; T.W.B. analyzed data; and T.W.B. and D.A.S. wrote the paper.

The authors declare no competing interest.

This article is a PNAS Direct Submission. M.E. is a guest editor invited by the Editorial Board.

[1]To whom correspondence may be addressed. Email: tbell@whoi.edu.

This article contains supporting information online at http://www.pnas.org/lookup/suppl/doi:10.1073/pnas.2105135118/-/DCSupplemental.

Published December 28, 2021.

and reproduction allows for the examination of many generational cycles relative to most terrestrial ecosystems (20). The macroscopic kelp sporophytes are formed from the sexual reproduction of two microscopic gametophytes, which germinate from recently settled zoospores on subtidal rocky reef (21). Supplied with sufficient light and nutrients (22), sporophytes can initiate hundreds of fronds and produce billions of zoospores over an individual's 1- to 7-y life span (23). As the fronds buoy to the surface to form the floating canopy, the resulting three-dimensional structure provides habitat to a diverse ecological community. Each kelp frond has a natural life span of ∼100 d, and under favorable conditions, new fronds are initiated to replace those lost through senescence (9). While age-dependent mortality accounts for most frond losses, frond elongation rate and persistence are sensitive to multiple environmental drivers including nutrient availability and wave disturbance, respectively (24).

As extrinsic environmental factors can synchronize plant functions over large scales (25, 26), regional giant kelp growth dynamics are typically associated with seasonal fluctuations in seawater nitrate concentration (27–29). In the coastal upwelling systems in which giant kelp is distributed, seawater nitrate concentrations are negatively and nonlinearly related to ocean temperatures and vary seasonally with cool, nutrient-rich surface waters during the spring upwelling season and warm, nutrient-poor conditions in the summer and fall (30). However, while declines in giant kelp abundance are often thought to be a function of wave disturbance (20, 21), reductions in canopy biomass are often variable in time across areas sheltered from large wave events (31) occurring months after seawater nitrate concentrations are depleted.

The chlorophyll *a* to carbon ratio (Chl:C, an established proxy for physiological condition for phytoplankton; ref. 32) is positively associated with kelp growth rate, frond initiation, and biomass accumulation (33, 34) and can be determined from aerial spectroscopic measurements (31). Increases in Chl:C are positively related to external environmental factors such as seawater nitrate concentration (34); however, photosynthetic performance is known to decrease with age, especially in a high light environment (35). Estimates of giant kelp physiology across space may elucidate patterns in growth and decline missed by measures of biomass dynamics alone.

To disentangle the roles of the environment and senescence on giant kelp dynamics, we investigated the spatiotemporal patterns of canopy physiological condition and biomass over regional (1 to 100 km) and local (10 m to 1 km) scales across a 4,000 km^2 study area in the Santa Barbara Channel (SBC), California, United States. We combine an unprecedented dataset of repeat imaging spectrometer data (two to three images per year, 2013 to 2015), over three decades of giant kelp canopy biomass and age determinations from Landsat satellites (>10 images per year, 1984 to 2017), and longitudinal field observations to characterize the processes regulating kelp abundance dynamics over multiple spatial scales.

Results

Remote sensing observations were used assess spatiotemporal patterns in seawater temperature and nutrient concentrations, giant kelp canopy biomass, and canopy Chl:C values. Seawater nitrate concentrations inside kelp forests were negatively and nonlinearly related to temperature, with nitrate concentrations falling below 1 μM (the nitrate concentration necessary for maximal kelp growth) at 14.1 to 14.5 °C and decreasing gradually as temperature increased (r^2 = 0.76, P < 0.001; *SI Appendix*, Fig. S1). Canopy biomass dynamics were estimated from multispectral satellite imagery using established techniques (36). The spectral Chl:C algorithm (31) produced accurate estimates of canopy Chl:C, as field-sampled frond Chl:C was strongly associated with Chl:C estimated from the spectral imagery ($y = 0.95x + 0.03$; r^2 = 0.67, P < 0.001; *SI Appendix*, Fig. S2).

Regional scale (1 to 100 km) kelp canopy Chl:C displayed considerable geographical variability across the SBC during the April and June image dates. For example, the June 2014 image showed a Chl:C range of 0.104 to 0.275 mg · mg^{-1} and was negatively related to sea surface temperature (r = −0.75, P < 0.001; Fig. 1 *A* and *B*). Over the study period (2013 to 2015), negative relationships were found between sea surface temperature and regional scale Chl:C for five of the eight image dates (Fig. 1*C* and *SI Appendix*, Table S1). The three dates that did not show significant relationships occurred when extreme temperature conditions were found for the SBC (Fig. 1*C*). Across all dates, the regional relationship between sea surface temperature and Chl:C was negative and nonlinear (r^2 = 0.47, P < 0.001; Fig. 1*C*) and mimicked results from field-sampled canopy blades (*SI Appendix*, Fig. S3; ref. 34). Regional scale Chl:C during the spring upwelling season (mean Chl:C in April 2013 to 2015) was also positively related to the long-term (34-y) mean annual kelp canopy persistence (r^2 = 0.20, P < 0.001; *SI Appendix*, Fig. S4).

Local scale (10 m to 1 km) variations in Chl:C for individual kelp forests often exceeded the range of regional scale Chl:C observed across the entire study area (Fig. 2). Local scale Chl:C determinations from individual image pixels (18 m) covering an example kelp forest canopy in the western SBC (Fig. 2*A*) were negatively associated with canopy age (Fig. 2 *C–H* and *SI Appendix*, Fig. S5*A*). Across single and multiple image dates, local scale Chl:C displayed a negative and nonlinear relationship with canopy age, with a fourfold decrease in Chl:C between canopy ages of 50 to 100 d (r^2 = 0.69, P < 0.001; Fig. 3*A*). Similar local scale patterns in Chl:C were found for other kelp forests showing comparable nonlinear relationships with canopy age (*SI Appendix*, Fig. S5). Chlorophyll pigment content of field-sampled canopy fronds across five frond cohorts showed analogous nonlinear declines with age (Fig. 3*B*). When chlorophyll content was normalized to account for the effect of different environmental conditions throughout the season, there was a consistent nonlinear pattern of pigment concentration decline (r^2 = 0.88, P < 0.001) that was similar to estimates from the spectral imagery (Fig. 3*C*).

Examples of spatial patterns of loss corresponding to growth patterns earlier in the growing season can also be found in the Landsat time series of canopy biomass (Fig. 4). Kelp canopy areas that emerged in the spring reached peak biomass at the same time as areas that emerged in the summer. However, the area of spring canopy emergence declined and was lost earlier than the canopy that emerged in the summer despite the absence of destructive wave events in the fall and winter.

Discussion

The regional scale relationship between frond Chl:C and seawater temperature (Fig. 1) has implications for the growth and persistence of giant kelp forests. Field studies show that Chl:C is positively related to seawater nitrate concentrations up to 1 μM and is positively correlated with changes in canopy biomass in southern California (34). This study also shows that declines in canopy Chl:C led to large reductions in net primary production in the following months (34). The observed decline in regional scale Chl:C begins between 14 and 15 °C, the temperature range associated with 1 μM seawater nitrate concentration, and reaches a minimum at 19 °C, when seawater nitrate concentrations are typically below detection (*SI Appendix*, Fig. S1). Enhanced physiological condition related to nutrient supply is linked to increased growth rate and production (33, 34) and is

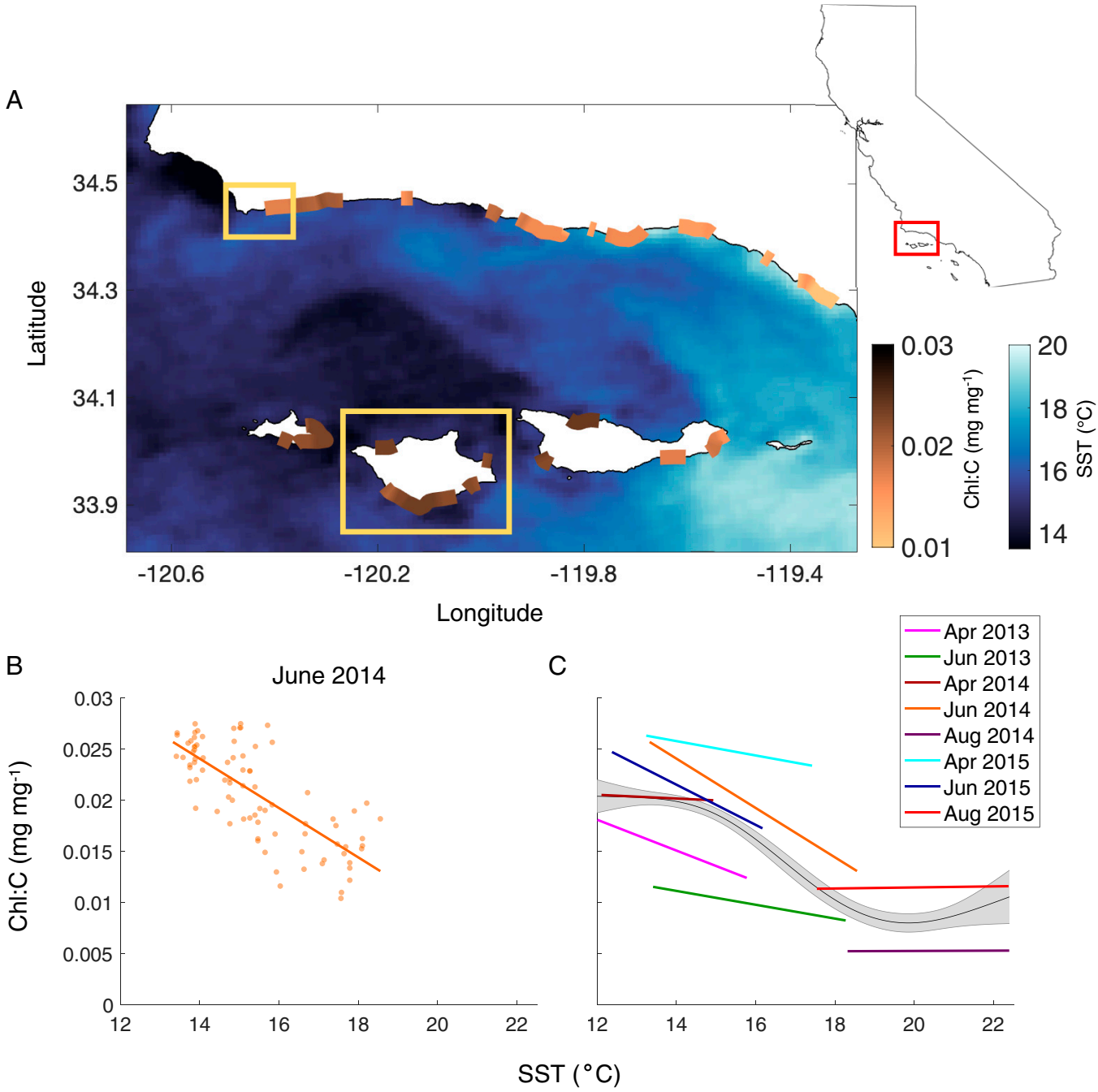

Fig. 1. (*A*) Regional-scale Chl:C and surface temperature in June 2014 for which the color of coastline represents the mean value of all remotely sensed Chl:C estimates over a 1-km scale. Yellow boxes show the location of the areas shown in Figs. 2 and 4. (*B*) Relationship between surface temperature and Chl:C for the June 2014 image. (*C*) The mean relationship between surface temperature and Chl:C across all image dates. The black curve represents the mean nonlinear relationship; the gray area represents 2× SE.

likely related to stable recruitment, as reproductive structures are proportionally largest during cool, and thus nutrient-rich, seawater conditions (37). Mean regional scale Chl:C retrievals during the spring upwelling season were positively related to multidecadal kelp forest persistence (*SI Appendix*, Fig. S4). This link between upwelling season Chl:C and decadal kelp persistence implies that nutrient availability underlies regional scale kelp persistence patterns.

The local scale variations in Chl:C at times exceeded the range of regional scale Chl:C observed across the entire study area (Fig. 2*D*). Nutrient-rich waters in the western SBC are rapidly exchanged through large kelp forests, as nutrient concentration observations made within and outside giant kelp forests are similar (refs. 38 and 39). Previous work in other regions has suggested that giant kelp nutrient uptake rates may be affected by ambient currents and mixing (40, 41). In the SBC, current speeds along the mainland coast typically increase in the late spring and summer months (42) and coincide with a reduction in seawater nutrient concentrations (Fig. 2*B*). Thus, it is unlikely that fine scale hydrodynamics have a large influence on the physiological condition patterns observed. Together, this implies that the local scale variability in canopy Chl:C observed

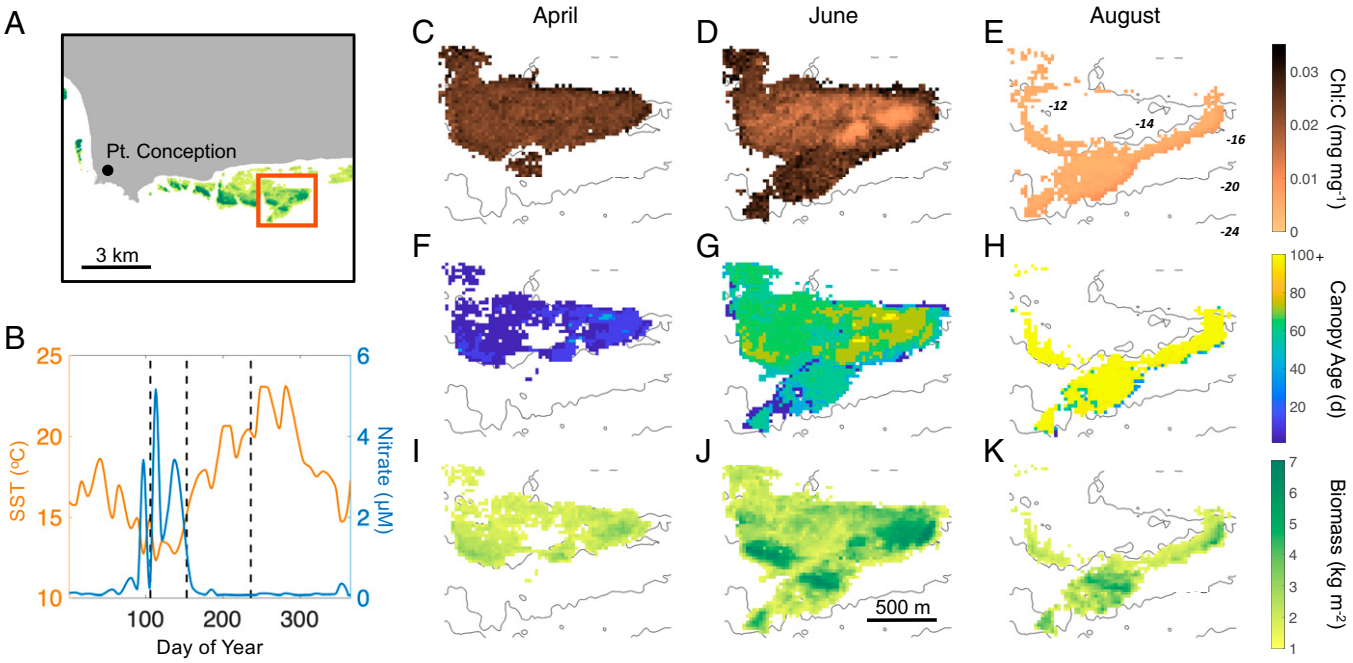

Fig. 2. (*A*) Western SBC with the large kelp forest highlighted in the red box. (*B*) Time series of sea surface temperature (orange line) and seawater nitrate concentration (blue line) near the kelp forest with hyperspectral image dates in 2015 shown as the dashed black lines. (*C–E*) Chl:C (AVIRIS, 18-m pixels), (*F–H*) canopy age, and (*I–K*) canopy biomass density (Landsat, 30-m pixels) for the kelp forest across the three dates. Black lines represent bathymetry (meters).

across a single image (Fig. 2*D* and *SI Appendix*, Fig. S5) was too large to be driven by local scale nutrient limitation, suggesting an alternate driver for local scale variations in Chl:C.

Local scale Chl:C was negatively associated with age across both single and multiple image dates with lower values found in older canopies (Fig. 2 *C–H*). The strong negative relationship between Chl:C and canopy age implies that intrinsic biotic processes, such as senescence, provide an explanation of local scale kelp population dynamics (Fig. 3*A*). A synthesis of kelp frond cohort survivorship observations (9) showed that frond loss rate reaches a maximum at an age of ∼100 d simultaneous with Chl:C reaching its minimum (Fig. 3*A*). This pattern is consistent with our field observations of multiple frond cohorts across the spring and summer in which chlorophyll concentration decreased dramatically at ∼50 d irrespective of ambient nitrate concentrations (Fig. 3 *B* and *C*). The sudden nonlinear decline in Chl:C with increasing age displayed the expected survivorship pattern of a senescing population (8) indicating that local scale reductions in physiological condition are associated with frond senescence and not nutrient availability.

The local scale dynamics of Chl:C reveal frond demographic patterns that presage canopy decline. Seasonally increased seawater nitrate concentrations promote recruitment and frond elongation to form a surface canopy, which presents a uniformly elevated Chl:C as the forest is dominated by young, vigorously growing fronds (Fig. 2 *C*, *F*, and *I*; refs. 22, 43, and 44). Over the following months, new fronds are initiated, and the canopy develops into a mixture of growing and senescing fronds, depressing the average Chl:C in older areas, while new individuals bearing younger fronds emerge along the edges of the canopy (Fig. 3 *D*, *G*, and *J*). The microscopic stages of giant kelp have high light requirements and are vulnerable to intraspecific competition through shading (22, 45). In a fully developed kelp canopy, the edges have higher benthic light levels enabling the growth of new recruits (45, 46). As warm water is advected into the SBC during the summer and kelp becomes nitrogen limited, the regional scale physiological condition of the canopy decreases, and frond initiation is reduced (34). The lack of new fronds replacing fronds lost due to senescence further decreases the mean Chl:C of the canopy (Fig. 2 *E*, *H*, and *K*). Canopy fronds make the largest contribution to production (47), simultaneously translocating photosynthate to promote the growth of subsurface juvenile fronds (48). The reduction of photosynthetic performance in aging fronds inhibits frond initiation, preventing new frond cohorts from reaching the surface and ultimately leading to a loss of canopy (35, 48).

Previous studies of giant kelp canopy dynamics have reported increasing stochasticity at scales less than ∼1 km, indicating that other ecological phenomena, such as mortality, dispersal, or recruitment, may be responsible for local abundance patterns (49). Cavanaugh et al. (25) described an exponential decrease in southern California kelp population synchrony within distances of 200 m that corresponded to the spatial patterns of recruitment. Giant kelp exhibits episodic reproductive synchrony (50), and the high light requirements of microscopic stages (22) favor recruitment at the edges and away from established canopy. Deeper areas of the reef may be provided with elevated summertime seawater nutrients from internal waves, fueling the growth and eventual canopy formation of the late season cohorts (39, 51). Spatially synchronous recruitment of kelp sporophytes may result in the synchronous decline in physiological condition and loss of canopy fronds later in the year, exposing the scales of these benthic processes to detection by aerial imagery. In kelp systems in which recruitment of sporophytes is spatially asynchronous, these patterns in senescence would be difficult to observe at the scales used in this study.

Although local scale giant kelp dynamics are primarily governed by senescence, frond growth is fundamentally linked to extrinsic environmental drivers. The physiological condition of newly matured fronds is a function of the external nutrient and light environment and is positively related to frond initiation, net primary production, and biomass accumulation (34). Elevated seawater nitrate concentrations lead to vigorous growth in the spring and early summer, producing dense kelp canopies

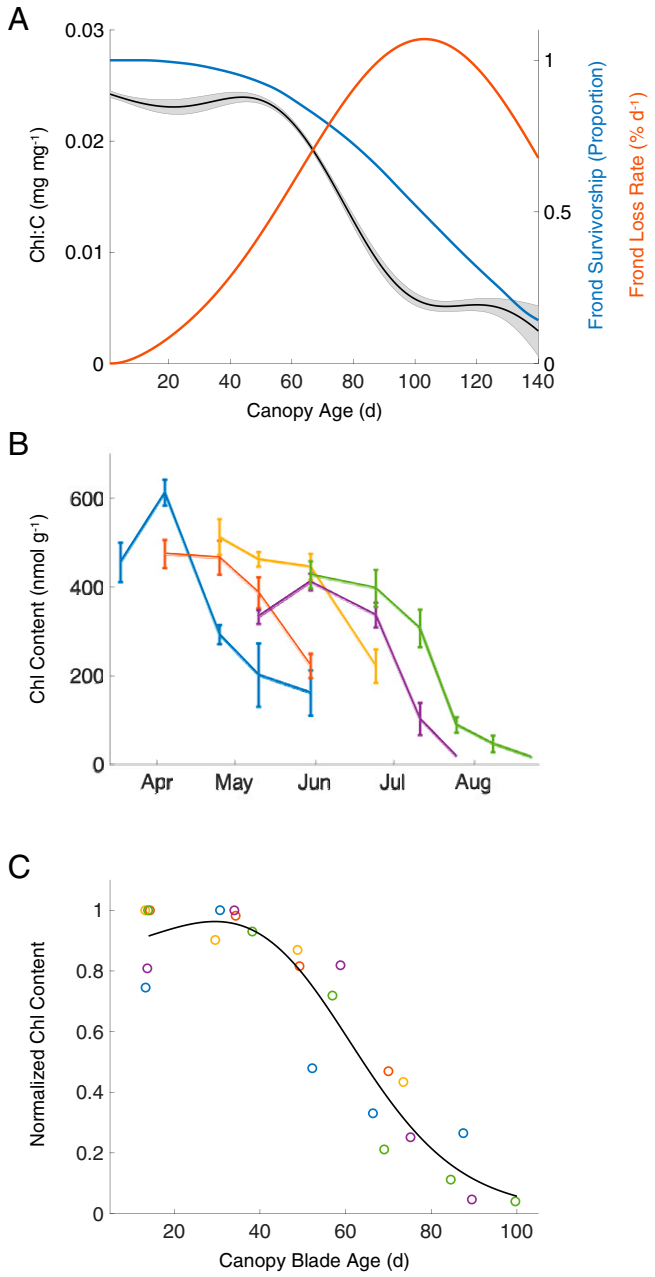

Fig. 3. (*A*) The nonlinear relationship between canopy age and Chl:C across all three image dates in 2015 for the large kelp forest in Fig. 2 (black curve; the gray shaded area represents 2× SE). The proportional frond survivorship (blue curve) and the loss rate of fronds (red curve) across three kelp forests in the SBC; synthesis of data from ref. 9. (*B*) Canopy chlorophyll *a* content as a function of age across five frond cohorts sampled in the SBC in 2019. Errors bars show SE. (*C*) The relationship between chlorophyll *a* content, normalized to the maximum of each frond cohort, and age for the five frond cohorts shown in *B*. Points are slightly jittered for visibility and colored to correspond to their respective frond cohort.

that reach maximum biomass shortly after seawater nitrate concentrations fall (Fig. 4 *A*–*D*; ref. 29). Since the life span of kelp fronds is generally unaffected by seawater nitrate conditions (9), reef areas that produce canopy earlier in the year will possess a greater proportion of older fronds and lose canopy at a faster rate in the subsequent months, especially in the absence of wave disturbance (Fig. 4 *B*, *E*, and *F*). Variable spatial patterns in frond demographics can lead to high standing biomass months after optimal growing conditions have passed, making it difficult to directly link regional nitrate conditions to local scale kelp dynamics (52). This is of particular importance, as marine heat waves and associated low-nutrient conditions have been implicated in the decline of kelp forests globally (53) with spatially diverse resilience patterns (54). While temperatures known to be deleterious to giant kelp were not observed during the hyperspectral time series at our focal site, significantly elevated temperatures were observed after the data shown in Fig. 2 and were associated with a complete loss of canopy. While the use of satellite imagery for monitoring kelp canopy dynamics is extensive, pixels are often binned at the regional scale, overlooking local scale dynamics captured by the imagery (55). Future studies should take advantage of this fine scale resolution to explore local patterns of resistance and resilience of these systems to high-temperature events.

Teasing apart the roles of the external environment and intrinsic biotic factors will aid in understanding plant population dynamics across ecosystems. Spatiotemporal estimates of physiological condition may benefit studies of lowland tropical forests and semiarid drylands due to the presence of many perennial evergreen species (15). Observations of plant physiology across scales will likely reveal spatial patterns of enhanced growth, stress, impending declines, and reproductive processes, such as inflorescence, missed by existing satellite sensors. Nascent repeat, global-scale imaging spectrometers open the possibility of simultaneously studying the physiology and abundance of populations, uncovering processes and patterns at a variety of scales, and giving ecologists a suite of powerful tools for disentangling the intrinsic and extrinsic factors regulating plant population dynamics.

Materials and Methods

Site Description. Portions of *Materials and Methods* appeared previously in ref. 56. The SBC covers an area of ~4,000 km^2 between the mainland coast of Santa Barbara and Ventura Counties, California, United States and the Northern Channel Islands (Fig. 1*A*). This region is influenced by the California Current, which transports cool, relatively fresh waters toward the equator to the west of the SBC, and the California Countercurrent that brings warm, saline waters into the eastern SBC (57). During the spring, upwelled water north of Point Conception is moved into the western areas of the Channel and leads to cool temperatures across the study region. In the early summer, warm waters are moved inshore from the east and create an east-to-west temperature gradient across the length of the SBC (30). Sea surface temperature (SST) dynamics in the SBC were assessed using 4-km resolution moderate resolution imaging spectroradiometer (MODIS) Aqua satellite sensor products (https://oceandata.sci.gsfc.nasa.gov/). The average SST for each 8-d period was assessed for the study period (June 2012 to December 2015; ref. 56). Relationships between temperature and seawater nitrate concentration were determined using data from five time series of nearshore CTD (conductivity, temperature, and depth) and bottle casts inside kelp forests in the SBC (58). A generalized additive model was used to model the nonlinear fit and predict seawater nitrate concentrations from the SST data using the mgcv package in R (59). To investigate the effect of nitrate uptake by kelp at the nearshore sites, this relationship was compared to the relationship derived from offshore bottle and CTD casts, and no significant difference was found (60). Daily maximum significant wave-height data were provided from the Coastal Data Information Program MOP version 1.1 model (ref. 61; cdip.ucsd.edu/MOP_v1.1).

Estimates of Kelp Canopy Biomass/Age. To track the development of giant kelp canopy, we estimated canopy biomass and age using Landsat 5, 7, and 8 multispectral imagery. Depending on the number of active Landsat sensors, an image is acquired every 8 to 16 d, with an average of one to two cloud-free images per month in this region. Landsat imagery has been used to track the dynamics of giant kelp canopy biomass across the coastline of California (19, 36). The fractional cover of kelp canopy was estimated for each 30 × 30 m pixel using multiple endmember spectral mixture analysis (MESMA; ref. 62), using 30 seawater spectral end-members unique to each image and one kelp canopy spectral end-member that does not change between image dates. The fractional cover of kelp canopy derived from the Landsat imagery was validated with a 15-y time series of diver-estimated kelp canopy biomass at multiple

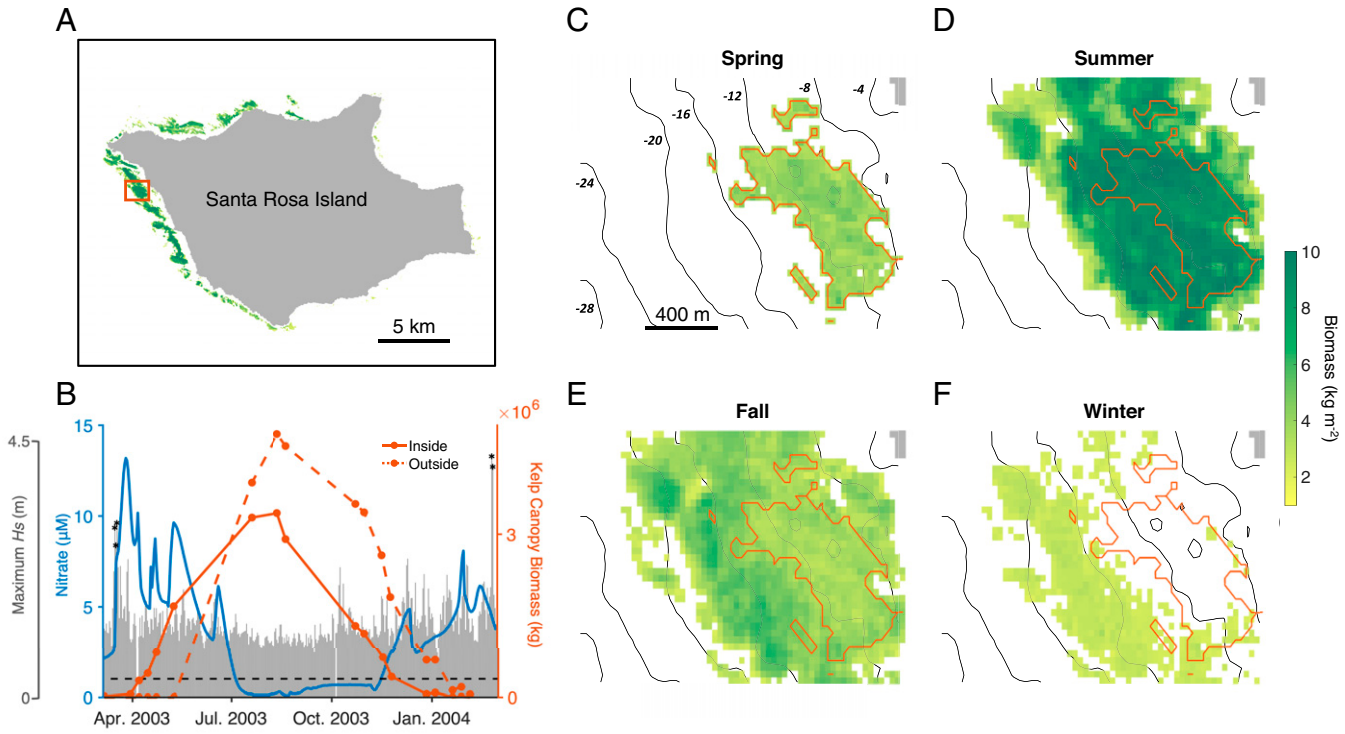

Fig. 4. (*A*) Giant kelp canopy biomass around Santa Rosa Island in summer 2003 with a section of kelp forest highlighted in the red box. (*B*) Annual time series of seawater nitrate concentration determined from sea surface temperature (blue line), maximum significant wave height (gray bars with large wave events shown with black asterisks), and kelp canopy biomass both inside (solid red line) and outside (dashed red line) the red polygon shown in *C*. Points along the canopy biomass lines show the dates of canopy biomass determinations using Landsat imagery. (*C–F*) Mean seasonal canopy biomass with red polygons showing the area where canopy was present in spring 2003. Black lines represent bathymetry (meters).

sites in the SBC ($r^2 = 0.64$, $P < 0.001$; refs. 36 and 63). We determined canopy age by setting the first image date on which canopy was observed in a pixel as age = 1 d. Long-term, annual kelp persistence was determined using a seasonal 34-y spatial time series of kelp canopy biomass from 1984 to 2017. Pixels were classified as occupied for a given year if kelp canopy was present at least once during that year. Persistence of an individual pixel was defined as the proportion of years that the pixel was occupied by kelp. Regional scale persistence was the mean annual occupancy of all pixels within the 1-km coastline segment.

Laboratory Analysis of Kelp Physiological Condition. Field samples of giant kelp canopy blade chlorophyll *a* pigment concentration and carbon content were taken at three kelp forest sites in the SBC: Arroyo Quemado (34.4677° N, 120.1191° W), Arroyo Burro (34.4003° N, 119.7446° W), and Mohawk (34.3941° N, 119.7296° W; ref. 34). Sites were sampled monthly over a 3-y period (August 2012 to August 2015). One mature blade (~14 d of age) was collected 2 m back from the tip of an actively growing frond from 15 different plants inside a permanent 40 × 40m plot. Blades were placed in a sealed plastic bag, which was immediately placed on ice in an opaque cooler. The blades were then transported to the laboratory, where they were stored at 4 °C until being processed within 24 h of collection. To examine changes in pigment concentration with canopy age, blades from frond cohorts were collected every 3 wk from March to September 2019 at Mohawk reef. A total of 100 fronds were tagged 2 m from the growing tip, and one blade from each of 10 different individuals was collected at the tag site. At each sampling period, one blade was sampled from 10 previously tagged fronds at the tag site, and an additional 100 fronds were tagged 2 m from the growing tip.

A 5-cm square was cut from the center of each blade ~5 cm above the pneumatocyst, and any epibionts were removed (blades usually had no epibionts). The reflectance of the square was then measured between 350 and 800 nm, at 1-nm intervals, using a Shimadzu UV-2401PC spectrophotometer with an integrating sphere attachment (56). Chlorophyll *a* concentration was determined from a 0.8-cm^2 disk excised from the center of each square. Each disk was weighed and placed in 4 mL dimethyl sulfoxide for 45 min at room temperature in the dark. The disk was then removed and washed with 1 mL water before being placed in 5 mL 3:1:1 acetone, methanol, and water solution for 2 h at 4 °C in the dark (56, 64). The extracts were placed in individual quartz cuvettes, and absorbance was measured between 350 and 800 nm using the spectrophotometer. Chlorophyll *a* concentration was determined using known absorbance-based equations (64). A separate 5-cm^2 disk was excised from each blade near the pneumatocyst and rinsed in a 10% HCl solution to remove any residual calcium carbonate from epibionts. These discs were weighed and combined for each site and date before being placed in a drying oven at 60 °C for several days, after which dry mass was recorded. The dried discs were ground to a fine powder and analyzed for carbon and nitrogen content using an elemental analyzer (Carlo-Erba Flash EA 1112 series, Thermo-Finnigan Italia). Chl:C was calculated by dividing the mass of chlorophyll *a* by the dry mass of carbon for each disk (56).

Hyperspectral Estimates of Kelp Canopy Physiological Condition. Giant kelp blade Chl:C was estimated using an algorithm developed from laboratory reflectance spectra of recently matured kelp blades (31). The 1-nm resolution laboratory reflectance spectra were degraded to ~10-nm bands consistent with the Airborne Visible/Infrared Imaging Spectrometer (AVIRIS). The difference in pseudoabsorbance (ln 1/Reflectance) between bands centered at 658 nm and 677 nm was related to the Chl:C of the kelp blades by Eq. **1**,

$$\text{Chl} : \text{C} = 0.0353e^{-7.53x}, \quad [1]$$

where x is equal to the difference in pseudoabsorbance between the two bands. Cross-validation analysis found that this relationship explained 76% of the observed variance in laboratory-assessed Chl:C (31).

The AVIRIS sensor provided hyperspectral image swaths (11-km width) of the SBC approximately three times per year (April, June, and August) from 2013 to 2015 as part of the HyspIRI Preparatory Airborne Campaign (https://hyspiri.jpl.nasa.gov/airborne). The AVIRIS sensor provides imagery of upwelling spectral radiance in 224 contiguous 10-nm bands (400 to 2,500 nm) at a pixel resolution of 18 m. For this study, orthocorrected level-2 reflectance products were used. All imagery is freely available (https://aviris.jpl.nasa.gov/).

The laboratory-derived giant kelp Chl:C algorithm (Eq. **1**) was then applied to the AVIRIS hyperspectral imagery of the SBC (65). Since each image pixel contains a mixture of giant kelp canopy and seawater, the fractional canopy cover determined by MESMA was used to exclude pixels with less than 10% canopy cover and to normalize the reflectance for the bands centered at 658 to 667 nm to the amount of kelp canopy present in each pixel. To validate the

algorithm for floating giant kelp canopy, we compared field-sampled Chl:C from each site to the mean Chl:C of the four AVIRIS pixels that overlaid each site for the sampling date closest to each image acquisition (*SI Appendix*, Fig. S2). If an image date fell between two field sample dates (>5 d), the later sampling date was used to account for changing environmental conditions. Field- and image-estimated Chl:C were compared using a reduced major axis least squares regression (56).

Relationship of Kelp Physiological Condition to Environmental Variables. To determine the relationship between SST and Chl:C estimated over regional scales, the coastline of the SBC was divided into 1-km segments. All kelp pixels were binned into their closest coastline segment. If the coastline segment contained >15 classified kelp pixels, the mean of those pixels was calculated and assigned to that segment for each image date. Each coastline segment was assigned a mean SST for each image date by taking the mean of all MODIS SST pixels within a 5-km radius for images between 2 and 20 d before the AVIRIS image date (56). Each segment's Chl:C and SST were compared using a linear regression across each image date. Since the overall relationship across all dates may not be linear, a generalized additive model was used to elucidate the potentially nonlinear fit using the mgcv package in R (59).

Data Availability. Time series data and derived imagery products have been deposited in the Environmental Data Initiative repository (https://doi.org/10.6073/pasta/89b63c4b49b80fb839613e9d389d9902) (63, 65).

ACKNOWLEDGMENTS. We thank Dan Reed, Kyle Cavanaugh, Max Castorani, Dana Morton, Jordan Snyder, Dylan Catlett, and Robert Miller for reviews of the manuscript. This work was supported by the US NSF (Grants OCE 1232779 and 1831937), by the US Department of Energy (Cooperative Agreement DE-AR0000922), and by NASA (Grant NNX14AR62A) and the NASA Earth and Space Sciences Fellowship program in support of T.W.B. Special thanks go to the HyspIRI Preparatory Airborne Campaign team.

1. S. A. Levin, The problem of pattern and scale in ecology. *Ecology* **73**, 1943–1967 (1992).
2. J. A. Wiens, Spatial scaling in ecology. *Funct. Ecol.* **3**, 385–397 (1989).
3. A. S. Watt, Pattern and process in the plant community. *J. Ecol.* **35**, 1 (1947).
4. R. H. Whittaker, Vegetation of the Great Smoky Mountains. *Ecol. Monogr.* **26**, 1–80 (1956).
5. M. G. Turner, V. H. Dale, R. H. Gardner, Predicting across scales: Theory development and testing. *Landsc. Ecol.* **3**, 245–252 (1989).
6. P. G. Jarvis, K. G. McNaughton, Stomatal control of transpiration: Scaling up from leaf to region. *Adv. Ecol. Res.* **15**, 1–49 (1986).
7. P. Monaghan, A. Charmantier, D. H. Nussey, R. E. Ricklefs, The evolutionary ecology of senescence. *Funct. Ecol.* **22**, 371–378 (2008).
8. A. C. Leopold, Senescence in plant development: The death of plants or plant parts may be of positive ecological or physiological value. *Science* **134**, 1727–1732 (1961).
9. G. E. Rodriguez, A. Rassweiler, D. C. Reed, S. J. Holbrook, The importance of progressive senescence in the biomass dynam of giant kelp (*Macrocystis pyrifera*). *Ecology* **94**, 1848–1858 (2013).
10. P. B. Reich *et al.*, Generality of leaf trait relationships: A test across six biomes. *Ecology* **80**, 1955–1969 (1999).
11. B. Clough, D. T. Tan, D. X. Phuong, D. C. Buu, Canopy leaf area index and litter fall in stands of the mangrove *Rhizophora apiculata* of different age in the Mekong delta, Vietnam. *Aquat. Bot.* **66**, 311–320 (1999).
12. J. L. Monteith, Evaporation and environment. *Symp. Soc. Exp. Biol.* **19**, 205–234 (1965).
13. E. Ranta, V. Kaitala, J. Lindström, H. Linden, Synchrony in population dynamics. *Proc. R. Soc. Lond. B Biol. Sci.* **262**, 113–118 (1995).
14. C. B. Field *et al.*, Mangrove biodiversity and ecosystem function. *Glob. Ecol. Biogeogr. Lett.* **7**, 3–14 (1998).
15. G. P. Asner, D. E. Knapp, C. B. Anderson, R. E. Martin, N. Vaughn, Large-scale climatic and geophysical controls on the leaf economics spectrum. *Proc. Natl. Acad. Sci. U.S.A.* **113**, E4043–E4051 (2016).
16. S. L. Ustin, D. A. Roberts, J. A. Gamon, G. P. Asner, R. O. Green, Using imaging spectroscopy to study ecosystem processes and properties. *Bioscience* **54**, 523–534 (2004).
17. National Academies of Sciences, Engineering, and Medicine, *Thriving on Our Changing Planet: A Decadal Strategy for Earth Observation from Space* (The National Academies Press, Washington, DC, 2018).
18. C. M. Lee *et al.*, An introduction to the NASA Hyperspectral InfraRed Imager (HyspIRI) mission and preparatory activities. *Remote Sens. Environ.* **167**, 6–19 (2015).
19. K. Cavanaugh, D. Siegel, D. Reed, P. Dennison, Environmental controls of giant kelp biomass in the Santa Barbara Channel, California. *Mar. Ecol. Prog. Ser.* **429**, 1–17 (2011).
20. D. C. Reed, A. Rassweiler, K. K. Arkema, Biomass rather than growth rate determines variation in net primary production by giant kelp. *Ecology* **89**, 2493–2505 (2008).
21. M. H. Graham, A. H. Buschmann, Global ecology of the giant kelp *Macrocystis*: From ecotypes to ecosystems. *Oceanogr. Mar. Biol. Annu. Rev.* **45**, 39–88 (2007).
22. L. Deysher, T. Dean, In situ recruitment of sporophytes of the giant kelp, *Macrocystis pyrifera* (L.) C. A. Agardh: Effects of physical factors. *J. Exp. Mar. Biol.* **103**, 41–63 (1986).
23. W. J. North, "Review of *Macrocystis* biology" in *Biology of Economic Algae*, I. Akatsuka, Ed. (Academic Publishing, The Hague, 1994), pp. 447–527.
24. D. C. Reed *et al.*, Wave disturbance overwhelms top-down and bottom-up control of primary production in California kelp forests. *Ecology* **92**, 2108–2116 (2011).
25. K. C. Cavanaugh *et al.*, Synchrony in dynamics of giant kelp forests is driven by both local recruitment and regional environmental controls. *Ecology* **94**, 499–509 (2013).
26. W. D. Koenig, J. M. H. Knops, Large-scale spatial synchrony and cross-synchrony in acorn production by two California oaks. *Ecology* **94**, 83–93 (2013).
27. V. A. Gerard, In situ rates of nitrate uptake by giant kelp, *Macrocystis pyrifera* (L.) C. Agardh: Tissue differences, environmental effects, and predictions of nitrogen-limited growth. *J. Exp. Mar. Biol. Ecol.* **62**, 211–224 (1982).
28. M. T. Brown, M. A. Nyman, J. A. Keogh, N. K. M. Chin, Seasonal growth of the giant kelp *Macrocystis pyrifera* in New Zealand. *Mar. Biol.* **129**, 417–424 (1997).
29. T. W. Bell, K. C. Cavanaugh, D. C. Reed, D. A. Siegel, Geographical variability in the controls of giant kelp biomass dynamics. *J. Biogeogr.* **42**, 2010–2021 (2015).
30. F. Henderikx Freitas, D. A. Siegel, S. Maritorena, E. Fields, Satellite assessment of particulate matter and phytoplankton variations in the Santa Barbara Channel and its surrounding waters: Role of surface waves. *J. Geophys. Res. Oceans* **122**, 355–371 (2017).
31. T. W. Bell, K. C. Cavanaugh, D. A. Siegel, Remote monitoring of giant kelp biomass and physiological condition: An evaluation of the potential for the Hyperspectral Infrared Imager (HyspIRI) mission. *Remote Sens. Environ.* **167**, 218–228 (2015).
32. E. Laws, T. Bannister, Nutrient and light-limited gowth of *Thalassiosira fluviatilis* in continuous culture, with implecations for phytoplankton growth in the ocean. *Limnol. Oceanogr.* **25**, 457–473 (1980).
33. M. Shivji, Interactive effects of light and nitrogen on growth and chemical composition of juvenile *Macrocystis pyrifera* (L.) C. At. (Phaeophyta) sporophytes. *J. Exp. Mar. Biol. Ecol.* **89**, 81–96 (1985).
34. T. W. Bell, D. C. Reed, N. B. Nelson, D. A. Siegel, Regional patterns of physiological condition determine giant kelp net primary production dynamics. *Limnol. Oceanogr.* **63**, 472–483 (2018).
35. G. E. Rodriguez, D. C. Reed, S. J. Holbrook, Blade life span, structural investment, and nutrient allocation in giant kelp. *Oecologia* **182**, 397–404 (2016).
36. T. W. Bell, J. A. Allen, K. C. Cavanaugh, D. A. Siegel, Three decades of variability in California's giant kelp forests from the Landsat satellites. *Remote Sens. Environ.* **238**, 110811 (2020).
37. D. C. Reed, A. Ebeling, T. W. Anderson, M. Anghera, Differential reproductive responses to fluctuating resources in two seaweeds with different reproductive strategies. *Ecology* **77**, 300–316 (1996).
38. G. A. Jackson, Nutrients and production of giant kelp, *Macrocystis pyrifera*, off southern California. *Limnol. Oceanogr.* **22**, 979–995 (1977).
39. J. P. Fram *et al.*, Physical pathways and utilization of nitrate supply to the giant kelp, *Macrocystis pyrifera*. *Limnol. Oceanogr.* **53**, 1589–1603 (2008).
40. C. L. Hurd, Water motion, marine macroalgal physiology, and production. *J. Phycol.* **36**, 453–472 (2000).
41. T. A. Stephens, C. D. Hepburn, Mass-transfer gradients across kelp beds influence *Macrocystis pyrifera* growth over small spatial scales. *Mar. Ecol. Prog. Ser.* **515**, 97–109 (2014).
42. M. R. Fewings, L. Washburn, J. C. Ohlmann, Coastal water circulation patterns around the Northern Channel Islands and Point Conception, California. *Prog. Oceanogr.* **138**, 283–304 (2015).
43. R. C. Zimmerman, J. N. Kremer, Episodic nutrient supply to a kelp forest ecosystem in Southern California. *J. Mar. Res.* **42**, 591–604 (1984).
44. R. C. Zimmerman, J. N. Kremer, In situ growth and chemical composition of the giant kelp, *Macrocystis pyrifera*: Response to temporal changes in ambient nutrient availability. *Mar. Ecol. Prog. Ser.* **27**, 277–285 (1986).
45. H. Stewart, J. Fram, D. Reed, Differences in growth, morphology and tissue carbon and nitrogen of *Macrocystis pyrifera* within and at the outer edge of a giant kelp forest in California, USA. *Mar. Ecol. Prog. Ser.* **375**, 101–112 (2009).
46. D. R. Schiel, M. S. Foster, The population biology of large brown seaweeds: Ecological consequences of multiphase life histories in dynamic coastal environments. *Annu. Rev. Ecol. Evol. Syst.* **37**, 343–372 (2006).
47. M. F. Colombo-Pallotta, E. García-Mendoza, L. B. Ladah, Photosynthetic performance, light absorption, and pigment composition of *Macrocystis Pyrifera* (Laminariales, Phaeophyceae) blades from different depths. *J. Phycol.* **42**, 1225–1234 (2006).
48. M. Fox, Biomass loss reduces growth and resource translocation in giant kelp *Macrocystis pyrifera*. *Mar. Ecol. Prog. Ser.* **562**, 65–77 (2016).
49. M. D. Donnellan, *Spatial and Temporal Variability of Kelp Forest Canopies in Central California* (San Jose State University, San Jose, CA, 2004).
50. D. C. Reed, T. W. Anderson, A. W. Ebeling, M. Anghera, The role of reproductive synchrony in the colonization potential of kelp. *Ecology* **78**, 2443–2457 (1997).
51. E. E. McPhee-Shaw *et al.*, Mechanisms for nutrient delivery to the inner shelf: Observations from the Santa Barbara Channel. *Limnol. Oceanogr.* **52**, 1748–1766 (2007).

52. M. A. Brzezinski *et al.*, Multiple sources and forms of nitrogen sustain year-round kelp growth on the inner continental shelf of the Santa Barbara channel. *Oceanography (Wash. D.C.)* **26**, 114–123 (2013).
53. T. Wernberg, K. Krumhansl, K. Filbee-Dexter, M. F. Pedersen, "Status and trends for the world's kelp forests" in *World Seas: An Environmental Evaluation*, Charles Sheppard, Ed. (Elsevier, 2019), pp. 57–78.
54. K. C. Cavanaugh, D. C. Reed, T. W. Bell, M. C. N. Castorani, R. Beas-Luna, Spatial variability in the resistance and resilience of giant kelp in southern and Baja California to a multiyear heatwave. *Front. Mar. Sci.* **6**, 413 (2019).
55. C. Butler, V. Lucieer, S. Wotherspoon, C. Johnson, Multi-decadal decline in cover of giant kelp *Macrocystis pyrifera* at the southern limit of its Australian range. *Mar. Ecol. Prog. Ser.* **653**, 1–18 (2020).
56. T. W. Bell, *Environmental Drivers of Giant Kelp Biomass and Physiological Condition through Space and Time*. (eScholarship, University of California, 2016).
57. S. Harms, C. D. Winant, Characteristic patterns of the circulation in the Santa Barbara Channel. *J. Geophys. Res. Oceans* **103**, 3041–3065 (1998).
58. L. Washburn, M. Brzezinski, C. Carlson, D. Siegel, SBC LTER: Ocean: Ocean currents and biogeochemistry: Nearshore water profiles (monthly CTD and chemistry) ver 23. Environmental Data Initiative (2019). https://doi.org/10.6073/pasta/b73d76d8d1465207be6d7fed19291fda. Accessed 8 November 2019.
59. S. N. Wood, *Generalized Additive Models: An Introduction with R* (Chapman and Hall, Boca Raton, FL, 2006).
60. J. N. Snyder, T. W. Bell, D. A. Siegel, N. J. Nidzieko, K. C. Cavanaugh, Sea surface temperature imagery elucidates spatiotemporal nutrient patterns and serves as a tool for offshore kelp aquaculture siting in the Southern California Bight. *Front. Mar. Sci.* **7**, 00022 (2020).
61. W. O'Reilly, C. B. Olfe, J. Thomas, R. Seymour, R. Guza, The California coastal wave monitoring and prediction system. *Coast. Eng.* **116**, 118–132 (2016).
62. D. Roberts *et al.*, Mapping chaparral in the Santa Monica Mountains using multiple endmember spectral mixture models. *Remote Sens. Environ.* **65**, 267–279 (1998).
63. T. Bell, K. Cavanaugh, D. Siegel, SBC LTER: Time series of quarterly NetCDF files of kelp biomass in the canopy from Landsat 5, 7 and 8, since 1984 (ongoing) ver 14. Environmental Data Initiative (2021). https://doi.org/10.6073/pasta/89b63c4b49b80fb839613e9d389d9902. Accessed 7 May 2021.
64. G. Seely, M. Duncan, W. Vidaver, Preparative and analytical extraction of pigments from brown algae with dimethyl sulfoxide. *Mar. Biol.* **12**, 184–188 (1972).
65. T. W. Bell, D. A. Siegel, Kelp canopy chlorophyll to carbon ratio derived from aerial hyperspectral imagery ver 1. Environmental Data Initiative (2021). 10.6073/pasta/c85974f3c0d11fb8cdb1ac2890698906. Accessed 7 August 2021.